Three-Dimensional Navier-Stokes Simulations of Non-Premixed Reactive Vortex Breakdown

Joseph D. Chung, Xiao Zhang, Carolyn R. Kaplan, and Elaine S. Oran
University of Maryland, Department of Aerospace Engineering
College Park, MD, USA

1 Introduction

Swirling jet flows appear in many forms in nature, such as tornadoes, hurricanes, dust devils, and fire whirls. They are used in combustion devices to mix fuel and air or to stabilize a flame. With the "right" conditions of swirl (ratio of azimuthal to axial velocity), adverse pressure gradient (aligned with the jet axis), and Reynolds number, swirling flows transition to a new state with a stagnation point and finite recirculation zone along the jet axis. This transition is referred to as vortex breakdown [1–3] and the resulting states have significant effects on the ensuing fluid and combustion dynamics.

The result of vortex breakdown has been described by three distinct states [1, 2]: the bubble mode, spiral mode, and double-helix mode. Due to computational constraints, early nonreactive, numerical simulations of vortex breakdown assumed incompressible, laminar, axisymmetric, and steady flows. These assumptions, however, do not allow the computation of the spiral and double-helix modes because of their inherent three-dimensional and unsteady structures [3, 4]. Later approaches solved the unsteady, three-dimensional, incompressible Navier-Stokes equations and were able to compute nonsymmetric modes of breakdown [5, 6]. For example, Spall et al. [5] studied the bubble mode of breakdown and its asymmetry. Ruith et al. [6] computed all three major modes by varying the Reynolds number, swirl, and jet profile.

Vortex breakdown has also been studied in reactive systems, primarily in swirl-stabilized premixed combustors. Huang and Yang [7] computed the flow within such a combustor by using three-dimensional, compressible large eddy simulations (LES) with a flamelet model (FM) and showed that increasing the swirl beyond a critical value can cause an upstream propagation of vortex breakdown. This was also shown by the LES-FM computations of Duwig and Fuchs [8], who also showed the formation of a helical mode.

Recent experiments by Xiao et al. [9] and Hariharan et al. [10] have shown the transition of a fire whirl into a flame which exhibits the characteristics of vortex breakdown. It begins as a swirling, sooty flame which burns a liquid hydrocarbon and then reaches a steady state with only blue luminescence, indicating soot-free burning. The luminescence of the transitional state suggests that helical breakdown modes are present and the steady-state suggests the bubble mode. The flow structure and mode of combustion of this blue flame, the blue whirl, are, however, still unknown.

This paper is a first step in understanding the flow and combustion states of the blue whirl . Here, we demonstrate that reactive vortex breakdown can be computed in a nonpremixed system. This is done by solving the three-dimensional (3D), unsteady, compressible, reactive Navier-Stokes (NS) equations coupled to a calibrated chemical-diffusive model for flames and energy release. The resulting flow and flame structure is presented and discussed.

2 Numerical Model

The numerical model solves the unsteady, compressible, reactive Navier-Stokes equations. The hyperbolic fluxes are computed using unsplit, fourth-order, flux-corrected transport. All parabolic fluxes are spatially discretized using a second-order, three-point central scheme. The diffusive fluxes include Fickian species diffusion, Fourier heat conduction, and Newtonian viscosity. The barely implicit correction (BIC) algorithm [11, 12] is used to remove the acoustic limit on the CFL time-step constraint, thereby removing the numerical expense of explicitly integrating the NS equations in a low-Mach-number flow. Further details on the integration procedure are discussed in [12].

We use a calibrated chemical-diffusive model (CDM) [13] to regulate the conversion of reactant to product and control the rate of heat release. The chemical parameters of the Arrhenius rate and heat of combustion are calibrated to reproduce the flame and thermal properties of heptane-air mixtures within a NS computation for varying stoichiometry. This calibration procedure is described in [13]. This work assumes a constant molecular weight of $30.6\ \mathrm{g/mol}$ for all species and a constant specific heat ratio of 1.19 for all species and temperatures.

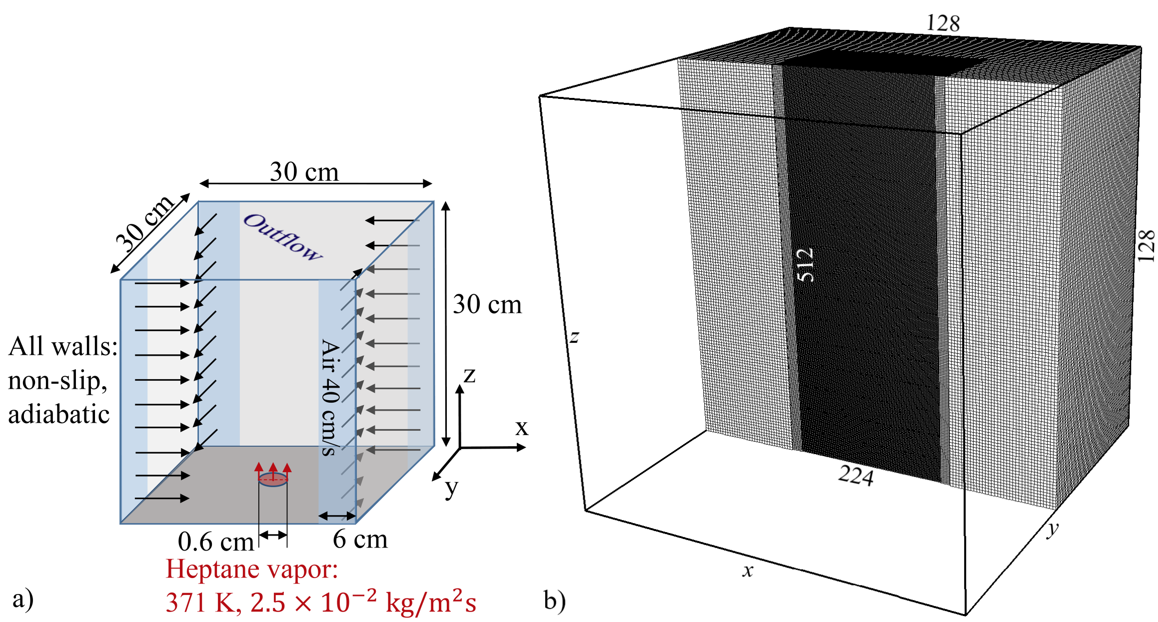

Figure 1: (a) The geometrical setup and boundary conditions. (b) A cut view of the computational mesh. The numbers indicate the number of cells at the coarsest and finest levels of refinement.

A schematic diagram of the geometrical setup and boundary conditions is shown in Fig. 1a. The domain is a cube with sides that are $30\ \mathrm{cm}$ long. The upper boundary is an outflow condition and all other boundaries are non-slip, adiabatic walls. A fuel that is representative of heptane vapor is injected within a $0.6\ \mathrm{cm}$ diameter at the center of the bottom wall with a constant flux of $2.5 \times 10^{-2}\ \mathrm{kg/m^2 s}$. The inflow fuel temperature is $371\ \mathrm{K}$, the evaporation temperature of heptane at $1\ \mathrm{atm}$. Circulation is applied by forcing air through the four corners along slits which are $6.0\ \mathrm{cm}$ wide. The inflow air is $298\ \mathrm{K}$ and its velocity is $40\ \mathrm{cm/s}$, orthogonal to the inflow boundary. The interior domain is initialized with quiescent air at $1\ \mathrm{atm}$ and $298\ \mathrm{K}$ with a column of hot product that is $1\ \mathrm{cm}$ in diameter and $10\ \mathrm{cm}$ high just above the fuel inflow for ignition. To avoid the generation of impulsive compression waves, the inflow of air and fuel are linearly accelerated from $0\ \mathrm{m/s}$ to their specified flux for the first $0.6\ \mathrm{s}$ of the computation.

The reactive BIC-FCT algorithm is incorporated into the BoxLib [14] adaptive mesh refinement library for parallelization and grid refinement. The mesh is Cartesian and each increasing level of refinement reduces the cell width by a half. In this current work, the mesh refinement is conducted in advance, based on the anticipated flow structure. The computational mesh is shown in Fig. 1b. The number of cells along the height and width of the coarsest and finest levels of refinement are also shown. In this work, the finest cell size is $\Delta x = 0.586\ \mathrm{mm}$. The time-step size is limited by the convective CFL condition, which is 0.3.

3 Results and Discussion

Center-slice contours of temperature, axial velocity, tangential velocity, and normalized pressure are shown in Fig. 2 at $5.6\ \mathrm{s}$, after the flow has reached a quasi-steady-state. In the early stages of the formation, the initial column of hot products are convected out of the domain due to buoyancy. This establishes an axial velocity profile which promotes the radial inflow of oxidizer towards the influx of fuel within the boundary layer. A diffusion flame is then established and grows wider until the circulation from the air inflow couples with the hot, low-density gas generated by the flame. A columnar vortex profile begins to form, and after $3.5\ \mathrm{s}$, the swirl intensity near the fuel inflow becomes strong enough to cause vortex breakdown just above the fuel inflow region. Then at $4\ \mathrm{s}$, the flame is lifted from the bottom floor as the radial inflow accelerates upward toward the axial direction. Figure 2a shows the lifted structure of the flame which is maintained for $2.5\ \mathrm{s}$. At $6.5\ \mathrm{s}$ the flame is no longer lifted and precesses around the edge of the fuel injection boundary. The average peak temperature of the flame is $2150\ \mathrm{K}$, approximately $150\ \mathrm{K}$ lower than the adiabatic flame temperature.

The computation shows the formation of two bubble modes. The first is defined by the finite reverse flow region in the center of the vortex axis just above the fuel inlet, shown as the blue region in the axial velocity contour of Fig. 2b. The bubble is surrounded by swirling gas. Most of the burning occurs within the lower half of this first bubble. Just outside of this reverse flow region, the axial velocity accelerates to $4\ \mathrm{m/s}$, showing that the flow is moving around it due to the blockage effect of the bubble. This is consistent with nonreactive characteristics of the bubble mode. Just above the first bubble, at a height of approximately $4\ \mathrm{cm}$, the peak tangential velocity moves closer to the vortex axis, showing the recovery of a columnar vortex. Here, the swirl is strong enough to generate another bubble mode at a height of $5\ \mathrm{cm}$. Above this second bubble, the bulk motion of the vortex attains a precessing columnar structure but becomes more turbulent.

The contour is shown in Fig. 2d shows the pressure normalized by $(P - P_{max})/(P_{max} - P_{min})$. The average value of $(P_{max} - P_{min})$ in the computation is $6.4\ \mathrm{Pa}$. The results show that the pressure is low near

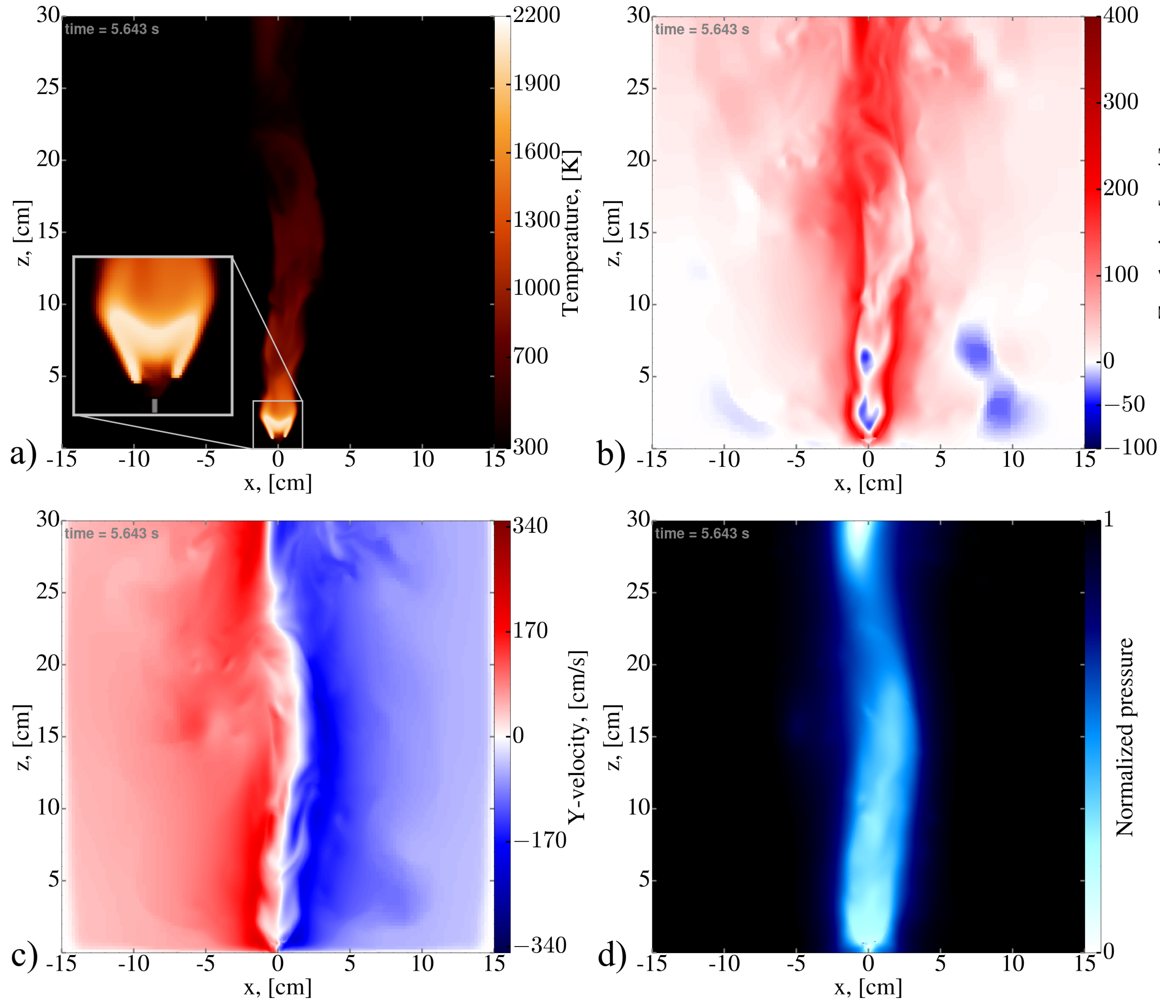

Figure 2: Contours of (a) temperature, (b) axial velocity, (c) tangential velocity, and (d) normalized pressure.

the core of the vortex and is higher away from it. This is consistent with what is observed in vortex flows and further shows that the computation has established a strongly swirling flow.

To better understand the burning properties of the flame, we compute the flame index,

$$\text{Flame index} = \frac{\nabla Y_{fuel} \cdot \nabla Y_{Oxidizer}}{|\nabla Y_{fuel}||\nabla Y_{oxidizer}|}, \tag{1}$$

where Y_{fuel} and $Y_{oxidizer}$ are the fuel and oxidizer mass fractions, respectively. The flame index is a measure of the angle between the fuel and oxidizer gradients. When the gradients are pointing towards each other, the flame index is negative and shows a diffusion flame. When the gradients point in the same direction, the flame index is positive and shows a premixed flame. The flame index is shown in Fig. 3 along with the contour of stoichiometric mixture fraction shown in black and heat release contours shown by colors. Red regions of flame index are positive and the blue regions are negative. Figure 3 shows that most of the heat release occurs near the bottom of the flame, but significant burning still occurs within the inner structure of the bubble and on the outside. The burning in the center is a premixed flame whereas the burning along the stoichiometric contour is a diffusion flame. A small region of premixed burning exists outside of the stoichiometric region, suggesting a triple flame structure. It is likely the flame structure here requires further grid refinement, which will be presented in a future work.

The velocity and flame structure suggests that most of the burning occurs due to diffusive mixing processes and not due to convective mixing from the bubble. All the fuel is burned in the lower half of the bubble, within a perimeter outside of the reverse flow region. The inner mixture of the bubble is fuel rich and the slow, recirculating flow within it increases the residence time of the fuel and provides sufficient time for it to diffuse towards the oxidizer in the outer part of the bubble.

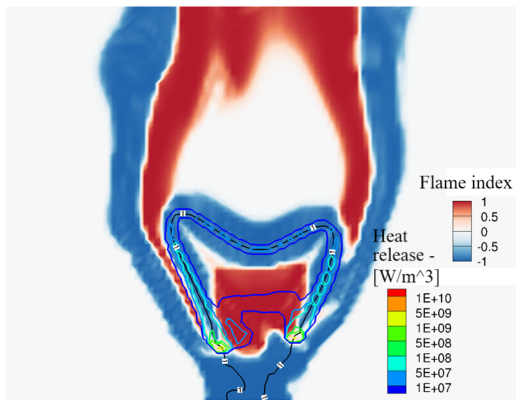

Figure 3: Contours of the flame index overlaid with contours of heat release within a zoomed in region of the reactive bubble.

4 Conclusions

This work has computed vortex breakdown and the resulting modes in a swirling diffusion flame by solving the unsteady, compressible, reactive NS equations. This computation has demonstrated the capability of a recently developed low-Mach-number solver and a calibrated chemical-diffusive model to compute the complex flow and flame structures of this flowfield. A fuel with burning properties of heptane was injected at the center of the bottom wall and circulation was applied by tangentially forcing air into the domain through four corners.

Two regions of vortex breakdown are observed, both exhibiting characteristics of the bubble mode. All the burning occurs within the lower half of the first bubble. The bubble traps a fuel-rich mixture inside of it. This fuel-rich mixture then continues to recirculate and diffuse excess fuel towards the oxidizer, causing most of the burning to occur within a diffusion flame. Computation of the flame index suggests that the burning occurs within a triple flame.

Acknowledgments

This work was supported by the Army Research Office (grant W911NF1710524) and by the National Science Foundation under award CBET 1839510. This work was also supported in part by the University of Maryland through Minta Martin Endowment Funds in the Department of Aerospace Engineering, the

Glenn L. Martin Institute Chaired Professorship, and the A. James Clark Distinguished Professorship at the A. James Clark School of Engineering. Computations were performed using the University of Maryland Deepthought2 HPC cluster. The first author is grateful to Dr. Vadim Gamezo and the Laboratory of Computational Physics, Naval Research Laboratory (NRL), for providing the DoD supercomputing resources to access Thunder. The authors also acknowledge the efforts of Dr. Ryan Houim, University of Florida, for his advice and assistance in the implementation of the algorithms.

References

[1] Sarpkaya T. (1971). On stationary and traveling vortex breakdowns. Journal of Fluid Mechanics 45: 545.

[2] Sarpkaya T. (1971). Vortex breakdown in swirling conical flows. AIAA Journal 9: 1792.

[3] Hall M. (1972). Vortex breakdown. Annual Review of Fluid Mechanics 4: 195.

[4] Grabowski WJ, Berger S. (1976). Solutions of the navier-stokes equations for vortex breakdown. Journal of Fluid Mechanics 75: 525.

[5] Spall R, Gatski T, Ash R. (1990). The structure and dynamics of bubble-type vortex breakdown. Proceedings of the Royal Society of London A: Mathematical, Physical and Engineering Sciences 429: 613.

[6] Ruith MR, Chen P, Meiburg E, Maxworthy T. (1966). Three-dimensional vortex breakdown in swirling jets and wakes: direct numerical simulation. Journal of Fluid Mechanics 486: 331.

[7] Huang Y, Yang V. (2005). Effect of swirl on combustion dynamics in a lean-premixed swirl-stabilized combustor. Proceedings of the Combustion Institute 30: 1775.

[8] Duwig C, Fuchs L. (2007). Large eddy simulation of vortex breakdown/flame interaction. Physics of Fluids 19: 075103.

[9] Xiao H, Gollner MJ, Oran ES. (2016). From fire whirls to blue whirls and combustion with reduced pollution. Proceedings of the National Academy of Sciences of the United States of America 34: 9457.

[10] Hariharan SB, Sluder ET, Gollner MJ, Oran ES. (2018). Thermal structure of the blue whirl. Proceedings of the Combustion Institute, In Press, Corrected Proof DOI: 10.1016/j.proci.2018.05.115

[11] Patnaik G, Guirguis RH, Boris JP, Oran ES. (1987) A barely implicit correction for flux-corrected transport. Journal of Computational Physics 71:1.

[12] Zhang X, Chung JD, Kaplan CR, Oran, ES. (2018). The barely implicit correction algorithm for low-Mach number flows. Computers & Fluids 175:230.

[13] Chung JD, Zhang X, Kaplan CR, Oran, ES. (2019) Low-Mach-number simulation of diffusion flames with the chemical-diffusive model. AIAA 2019-2169

[14] Center for Computational Sciences and Engineering, University of California, Berkeley, available at https://ccse.lbl.gov/index.html (Retrieved 10-2017).